Korean J. Chem. Eng., 33(5), 1599-1605 (2016)
DOI: 10.1007/s11814-015-0270-0

pISSN: 0256-1115
eISSN: 1975-7220

V-promoted Ni/Al_2O_3 catalyst for synthetic natural gas (SNG) production: Catalyst preparation methodologies

Qing Liu*, Fangna Gu*, Ziyi Zhong, Guangwen Xu*, and Fabing Su*,†**

*State Key Laboratory of Multiphase Complex Systems, Institute of Process Engineering, Chinese Academy of Sciences, Beijing 100190, China
**Institute of Chemical Engineering and Sciences, A*star, 1 Pesek Road, Jurong Island 627833, Singapore
(*Received 28 September 2015 • accepted 4 December 2015*)

Abstract−The effect of preparation method on the catalytic performance of V-promoted Ni/Al_2O_3 catalysts for synthetic natural gas (SNG) production via CO methanation has been investigated. The $Ni\text{-}V/Al_2O_3$ catalysts were prepared by co-impregnation (CI) method, deposition precipitation (DP) method as well as two sequential impregnation (SI) methods with different impregnation sequence. Among the prepared catalysts, the one prepared by CI method exhibited the best catalytic performance due to its largest H_2 uptake and highest metallic Ni dispersion. In a 91h-lifetime test, this catalyst showed high stability at high temperature and weight hourly space velocity. This work demonstrates that the catalytic performance of the V-promoted Ni/Al_2O_3 catalysts can be improved by carefully controlling the preparation method/conditions.

Keywords: CO Methanation, Synthetic Natural Gas (SNG) Production, Ni/Al_2O_3 Catalyst, Vanadium Oxide, Preparation Method

INTRODUCTION

To improve the effectiveness and cleanliness in the use of fossil energy sources, the production of synthetic natural gas (SNG) via methanation reaction ($CO+3H_2 \rightarrow CH_4+H_2O$) of syngas is a reasonable and feasible technical route to utilize the coal resources, particularly in regions or countries such as China with scarce natural gas but abundant coal resources [1,2]. Generally, Ni-based catalysts have been extensively used in methanation reaction due to their relatively high activity and low cost [3]. However, these catalysts often suffer from poor low-temperature activity; thus, a high reaction temperature (above 320 °C) is generally required to achieve the maximum CO conversion at atmospheric pressure [4]. Various promoters [2,5], supports [6-8] and preparation methods [9,10] have been tested to overcome this limit, but few of them show satisfactory activity at atmospheric-pressure at as low as ca. 300 °C.

In general, catalyst preparation methods and conditions have an important impact on the catalytic performance of a heterogeneous catalyst, as they are able to alter chemical and physical properties, such as surface area, particle size, particle distribution, and electronic structure of the catalyst. Hence, preparation methods and conditions should be carefully optimized in catalyst preparation. Recently, we found vanadium oxide is an effective promoter for supported-Ni-catalyst to improve the CO and CO_2 methanation reactions [11,12]. In continuation of our previous work, we prepared the $Ni\text{-}V/Al_2O_3$ catalysts by co-impregnation (CI) method, deposition precipitation (DP) method and two sequential impregnation (SI) methods with different impregnation sequence. The catalytic performance was evaluated and structures of the catalysts were characterized, and the results show that the H_2 uptake and metallic Ni dispersion of the catalysts are very sensitive to the preparation method, which are crucial for the high catalytic performance of catalysts in CO methanation reaction.

†To whom correspondence should be addressed.
E-mail: fbsu@ipe.ac.cn

EXPERIMENTAL

1. Preparation of Catalyst

All the chemicals with analytical grade including nickel (II) nitrate hexahydrate ($Ni(NO_3)_2 \cdot 6H_2O$), KOH and ethanol were purchased from Sinopharm Chemical Reagent Co. Ltd., China, and used without further treatment. Vanadyl (IV) acetylacetonate was purchased from Acros Organics. The commercial porous $\gamma\text{-}Al_2O_3$ (Zibo Honghe Chemical Co. Ltd., China) with a surface area of 164 $m^2\ g^{-1}$ was calcined at 400 °C in air for 2 h before use. The amounts of NiO and vanadium were fixed at 20 and 5 wt%, respectively.

20NA5V-SI-N (sequential impregnation method I): First, the $NiO/\gamma\text{-}Al_2O_3$ catalyst was prepared by wet impregnation method. The stoichiometric quantity of $Ni(NO_3)_2 \cdot 6H_2O$ was dissolved in ethanol, followed with addition of the $\gamma\text{-}Al_2O_3$ support to form a slurry. The slurry was vigorously stirred at room temperature overnight, and then heated to 70 °C to evaporate the liquid, followed with drying at 100 °C for 24 h and further calcination at 500 °C for 2 h in air with the heating rate of 2 °C min^{-1}. The collected catalyst with a NiO loading of 20 wt% was denoted as 20NA. Subsequently, the stoichiometric quantity of vanadyl (IV) acetylacetonate was dissolved in ethanol, followed with addition of 20NA to form a slurry.

After drying and calcination under the same conditions as 20NA, the finally obtained sample was denoted as 20NA5V-SI-N.

20NA5V-SI-V (sequential impregnation method II): The sample was prepared by the sequential impregnation method with impregnation vanadium species first and then nickel species. All the steps were the same as the above method, and the obtained sample was denoted as 20NA5V-SI-V.

20NA5V-CI (co-impregnation method): The sample was prepared by co-impregnation method. The procedure was the same as that of NiO/Al_2O_3 except that stoichiometric quantities of $Ni(NO_3)_2 \cdot 6H_2O$ and vanadyl (IV) acetylacetonate were dissolved in ethanol simultaneously. The obtained samples were denoted as 20NA5V-CI.

20NA5V-DP (deposition precipitation method): 1.00 g of the Al_2O_3 powder (>200 mesh) was added to 250 mL of distilled water, and the resulting mixture was thoroughly dispersed by ultrasonic treatment for 0.5 h. The obtained slurry was slowly heated to 80 °C in a water-bath under vigorous stirring. Subsequently, 0.005 M vanadyl (IV) acetylacetonate ethanol solution, 0.1 M $Ni(NO_3)_2$ aqueous solution and 0.1 M KOH aqueous solution were concurrently added to control the pH value at around 9.0. After aging for 6 h, the product was collected by filtration, washed twice with distilled water and ethanol, and dried at 100 °C in air, and finally calcined at 500 °C for 2 h with a heating rate of 2 °C min^{-1}. The obtained sample was denoted as 20NA5V-DP.

2. Catalysts Characterization

N_2 adsorption at −196 °C was measured by using a Quantachrome surface area & pore size analyzer NOVA 3200e. Prior to the measurement, the sample was degassed at 200 °C for 4 h under vacuum. The specific surface area was determined according to the Brunauer-Emmett-Teller (BET) method.

X-ray diffraction (XRD) patterns were recorded on a PANalytical X'Pert PRO MPD with a step of 0.02° using the Cu Kα radiation (λ=1.5418 Å) at 40 kV and 40 mA, and checked with the card number of Joint Committee on Powder Diffraction Standards (JCPDS). The crystal size of the sample was calculated using the Debye-Scherrer equation.

The exact composition of the catalysts was determined by Thermo Scientific iCAP 6300 inductively coupled plasma atomic emission spectrometry (ICP-AES).

H_2 temperature-programmed reduction (H_2-TPR), H_2 temperature-programmed desorption (H_2-TPD) and CO temperature-programmed desorption (CO-TPD) were carried out on a Quantachrome Automated chemisorption analyzer (chemBET pulsar TPR/TPD). For H_2-TPR, 0.05 g sample was loaded in a quartz U-tube and heated from room temperature to 200 °C at 10 °C min^{-1} and maintained for 1 h under He flow. Then, the sample was cooled to room temperature, followed by heating to 1,000 °C at 10 °C min^{-1} under a binary gas (10.0 vol% H_2/Ar) with a gas flow of 30 mL min^{-1}.

For H_2-TPD, 0.2 g catalyst was used and reduced in situ at 600 °C for 2 h by H_2/Ar flow previously. Then the sample was cooled to room temperature and saturated with H_2. After the physically adsorbed H_2 was removed by purging with Ar for 2 h, the sample was heated to 1,000 °C ramping at 10 °C min^{-1} in Ar flow (30 mL min^{-1}). The consumed or desorbed H_2 was detected continuously as a function of increasing temperature using a thermal conductivity detector (TCD). The dispersion of Ni was calculated by using the volume of chemisorbed H_2 based on the following formula described in our previous work [13].

$$D(\%) = \frac{2 \times V_{ad} \times M \times SF}{m \times P \times V_m \times d_r} \times 100$$

where V_{ad} (mL) represents the volume of chemisorbed H_2 at standard temperature and pressure (STP) conditions measured in the TPD procedure; m is the sample weight (g); M is the molecular weight of Ni (58.69 g mol^{-1}); P is the weight fraction of Ni in the sample determined by ICP; SF is the stoichiometric factor (the Ni : H molar ratio in the chemisorption) which is taken as 1, and V_m is molar volume of H_2 (22,414 mL mol^{-1}) at STP; d_r is the reduction degree of nickel calculated based on H_2-TPR results.

For CO-TPD, 0.20 g sample was pre-reduced in situ by H_2/Ar at 600 °C for 2 h, followed with adsorption of CO in 10 vol% CO/Ar sorption at room temperature for 0.5 h. After physically adsorbed CO was removed by purging with He for 1 h, the sample was heated to 550 °C at 10 °C min^{-1} in He flow (30 mL min^{-1}).

The microscopic features of the samples were observed by field emission scanning electron microscope (SEM) (JSM-6700F, JEOL, Japan) and transmission electron microscopy (TEM) (JEM-2010F, JEOL, Japan). Before the TEM measurement, the H_2-reduced catalysts were cooled to room temperature in an H_2 flow and then passivated in 1.0 vol% O_2/Ar gas mixture for 30 min to prevent bulk oxidation of the Ni nanoparticles.

3. Catalytic Measurement

Following our previous work [13], the CO methanation reaction was carried out in a fixed bed reactor at 0.1 MPa with a quartz tube. The influence of mass transfer had been examined and eliminated before the catalytic tests. First, 0.1 g catalyst sample (20-40 mesh) diluted with 5.0 g quartz sands (20-40 mesh) was uploaded in a quartz tube with an inner diameter of 8 mm. A thermocouple was inserted into the furnace chamber and bonded to the outside of the reactor tube near the middle position of the catalyst bed to control the reaction temperature. The catalyst was reduced at 600 °C in pure H_2 (100 mL min^{-1}) for 2 h and then cooled to the starting reaction temperature in H_2. The mixed H_2 and CO as well as N_2 (as an internal standard) were introduced into the reactor at a molar ratio of $H_2/CO/N_2$=3/1/1. The outlet gas stream from the reactor was cooled with a cold trap. Inlet and outlet gases were analyzed on line by Micro GC 3000A (Agilent Technologies). The gases of H_2, N_2, CH_4 and CO in gas products were separated by a molecular sieve column and detected by a TCD detector, while the CO_2, C_2H_4, C_2H_6, C_3H_6 and C_3H_8 gases were analyzed by another TCD with a Plot Q column. The CO conversion and CH_4 selectivity are defined as follows:

$$\text{CO conversion: } X_{CO}(\%) = \frac{F_{CO,\,in} - F_{CO,\,out}}{F_{CO,\,in}} \times 100$$

$$\text{CH}_4\text{ selectivity: } S_{CH_4}(\%) = \frac{F_{CH_4,\,out}}{F_{CO,\,in} - F_{CO,\,out}} \times 100$$

$$\text{CH}_4\text{ yield: } Y_{CH_4}(\%) = \frac{X_{CO} \times S_{CH_4}}{100} = \frac{F_{CH_4,\,out}}{F_{CO,\,in}} \times 100$$

Here, X is the conversion of CO, S is the selectivity of CH_4, Y is the yield of CH_4, $F_{i,\,in}$ and $F_{i,\,out}$ are the volume flow rates of species i (i=CO or CH_4) at the inlet and outlet.

Table 1. Physical and chemical properties of the samples

Catalysts	S_{BET}[a] ($m^2\ g^{-1}$)	V[b] ($cm^3\ g^{-1}$)	NiO content (wt%)[c]	V_2O_5 content (wt%)[c]	Ni particle size (nm)		H_2 uptake ($\mu mol\ g^{-1}$)	D[f] (%)
					XRD[d]	TEM[e]		
20NA5V-SI-N	132	0.32	19.11	5.10	11.2	12.8	102.9	7.7
20NA5V-SI-V	133	0.33	19.32	4.98	7.4	7.2	147.8	11.0
20NA5V-CI	144	0.33	20.10	4.90	<5.0	3.9	240.1	17.9
20NA5V-DP	200	0.49	19.85	5.05	5.1	4.9	191.1	14.2

[a]Surface area of the calcined sample derived from BET equation
[b]Pore volume of the calcined sample obtained from the volume of nitrogen adsorbed at the relative pressure of 0.97
[c]The exact composition of the calcined catalysts was determined by ICP-AES
[d]Particle size estimated from the XRD diffraction peak (2θ=44.6) using the Debye-Scherrer equation. Considering the limitation of this calculation method, the Ni particle size was denoted as '<5.0' when the calculated value was smaller than 5.0 nm
[e]The average particle size estimated from the TEM images
[f]Ni dispersion calculated from the H_2-TPR and H_2-TPD results

RESULTS AND DISCUSSION

1. Characterization of the Catalysts

Table 1 compiles the surface areas and pore volumes of the catalysts obtained from the N_2 adsorption (not shown here). The specific surface areas and total pore volumes of the catalysts prepared by different impregnation methods are almost the same, while those of 20NA5V-DP are much larger, which may be because the deposition of some NiO and V_2O_5 nanoparticles can make the surface of catalyst much coarser. In addition, the exact compositions of the above catalysts were determined by ICP-AES, which showed that the real NiO and V_2O_5 loadings of different catalysts were quite similar; and the Ni loading of 20NA5V-SI-N was slightly lower than 20 wt% due to the addition of V_2O_5 to 20NA (Table 1).

Fig. 1 shows the XRD patterns of both the calcined and the reduced catalysts prepared by different methods. As seen in Fig. 1(A), there is no appearance of any peaks corresponding to V_2O_5 in all the XRD patterns of the calcined catalysts due to the high dispersion status of vanadium species, which is similar to our previous work [11,12]. However, the NiO peak intensities of the catalysts prepared by SI method are very strong, while for the catalysts prepared by CI and DP methods, no NiO diffraction peaks can be observed, which indicates the high dispersion of NiO or the formation of NiO-V_2O_5 composite oxide ($Ni_3V_2O_8$) over the catalyst is significantly affected by different preparation methods. It was found that $Ni_3V_2O_8$ was formed during the calcination of the Ni-V/Al_2O_3 catalysts, which would result in the formation of smaller Ni particle sizes (<5.0 nm). Obviously, the dispersion and distribution of NiO and V_2O_5 over CI- and DP-made catalysts are quite similar to each other, resulting in the formation of more $Ni_3V_2O_8$ and highly dispersed oxidized nickel species. In contrast, less $Ni_3V_2O_8$ but more isolated NiO nanoparticles were formed over the SI-made catalysts, which led to the agglomeration of NiO. Accordingly, after reduction in H_2 flow, for 20NA5V-CI and 20NA5V-DP, small metallic Ni particle sizes were obtained, while those in the SI-made catalysts were larger (Fig. 1(B)), and among them, 20NA5V-CI has the smallest Ni particle size (<5 nm, Table 1).

As seen in Fig. 2(A), all the catalysts exhibit similar H_2-TPR profiles. Two distinct reduction peaks are observed: the first one appears in the range of 374-414 °C corresponding to the reduc-

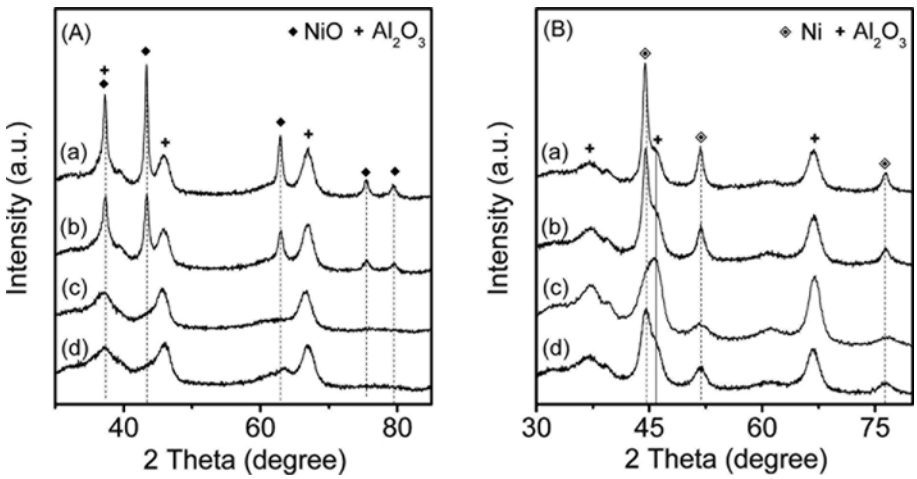

Fig. 1. XRD patterns of the calcined catalysts (A) and the reduced catalysts (B): (a) 20NA5V-SI-N, (b) 20NA5V-SI-V, (c) 20NA5V-CI, and (d) 20NA5V-DP.

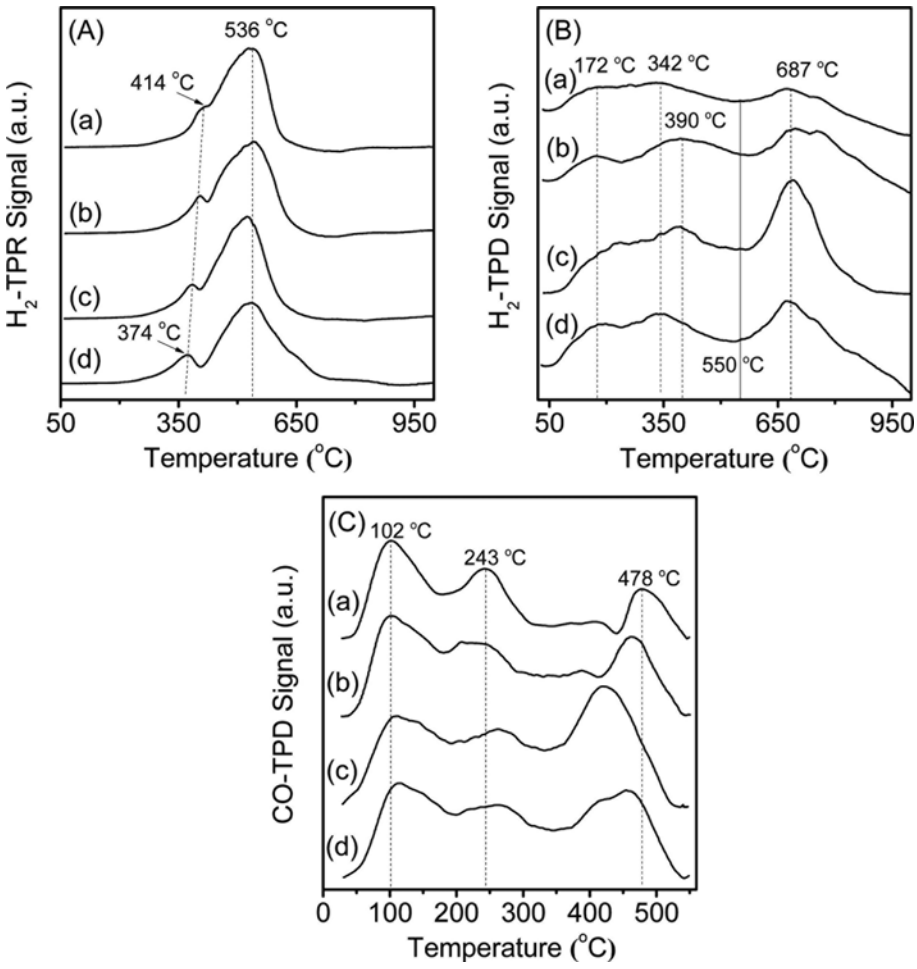

Fig. 2. H_2-TPR profiles (A), H_2-TPD profiles (B) and CO-TPD profiles (C) of the catalysts: (a) 20NA5V-SI-N, (b) 20NA5V-SI-V, (c) 20NA5V-CI, and (d) 20NA5V-DP.

tion of V_2O_5 to V_2O_3 [13,14], while the latter broad peak at 536 °C is assigned to the reduction of NiO species with middle strength of interaction with the support [2,5]. The shift of V_2O_5 reduction peak in the range of 374-414 °C indicates that the dispersion of V_2O_5 and interaction between V_2O_5 and NiO/Al_2O_3 composites vary from different preparation methods. In contrast, the NiO over different catalysts (seen in Fig. 2(A)) has similar interaction with the Al_2O_3 support.

H_2-TPD was performed to obtain insight into the effect of dissociative hydrogenation on the reaction activity of the catalysts. As seen in Fig. 2(B), three main H_2 desorption peaks are located in the H_2-TPD profiles of all the catalysts at around 172, 342 (or 390) and 687 °C, respectively. The first peak at low temperature is attributed to the chemisorbed hydrogen on the highly dispersed Ni nanoparticles having a large density of surface defects, which often serve as traps for surface hydrogen diffusion that can reduce the activation energy of hydrogen dissociation [11,15]. The second peak located at 342 (or 390) °C can be derived from the H_2 adsorbed on bulk or lowly-dispersed Ni nanoparticles [15]. While the third peak located at 687 °C can be assigned to the H_2 adsorbed in the subsurface layers of Ni atoms and/or to the spill-over H_2 [11,16]. Obviously, the profiles of different catalysts are similar, while there is an obvious change in the integrated areas with decreasing order of 20NA5V-CI>20NA5V-DP>20NA5V-SI-V>20NA5V-SI-N. In addition, the H_2 uptakes and the dispersion of Ni are calculated based on the H_2-TPD (below 550 °C) and H_2-TPR results and listed in Table 1, because 550 °C can be seen as the demarcation line between the peak 342 °C and the peak 687 °C in the H_2-TPD profiles (Fig. 2(B)). Although all the catalysts have the same composition, the measured H_2 uptakes and Ni dispersions vary greatly with different preparation methods and conditions, in which 20NA5V-CI has the highest total H_2 uptake of 240.1 μmol g^{-1} and Ni dispersion of 17.9% due to its smallest Ni particle size. These results reveal that the preparation methods are very crucial for the H_2 uptakes and the dispersion of Ni.

In CO methanation reaction, besides the hydrogenation of $*CH_x$ species, the dissociation of *CO is also crucial to the catalytic performance of a catalyst [17,18]. To investigate the effect of the preparation method on the CO sorption, CO-TPD was carried out over different catalysts (see Fig. 2(C) for results). The CO-TPD profiles of all the catalysts look similar and exhibit three main CO desorption peaks located at around 102, 243 and 478 °C, respectively, suggesting the presence of similar absorption sites in these catalysts. Among them, the peak at the low temperature (102 °C) represents

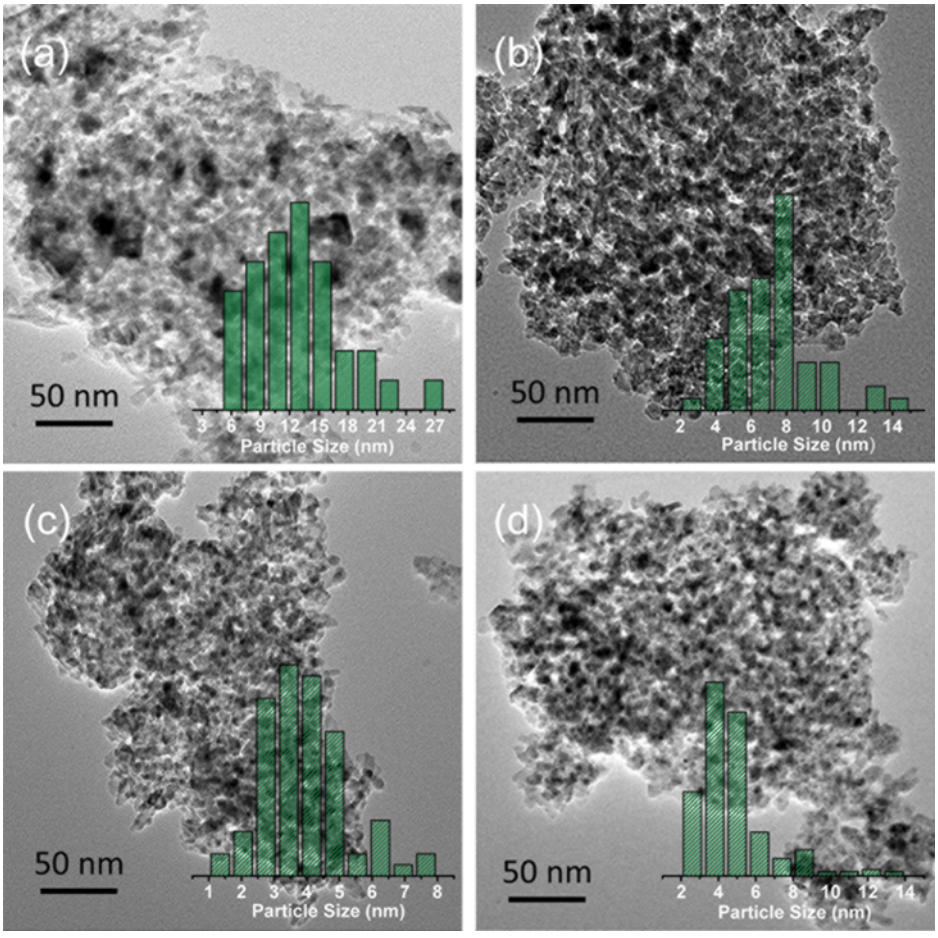

Fig. 3. TEM images of the reduced catalysts: (a) 20NA5V-SI-N, (b) 20NA5V-SI-V, (c) 20NA5V-CI, and (d) 20NA5V-DP.

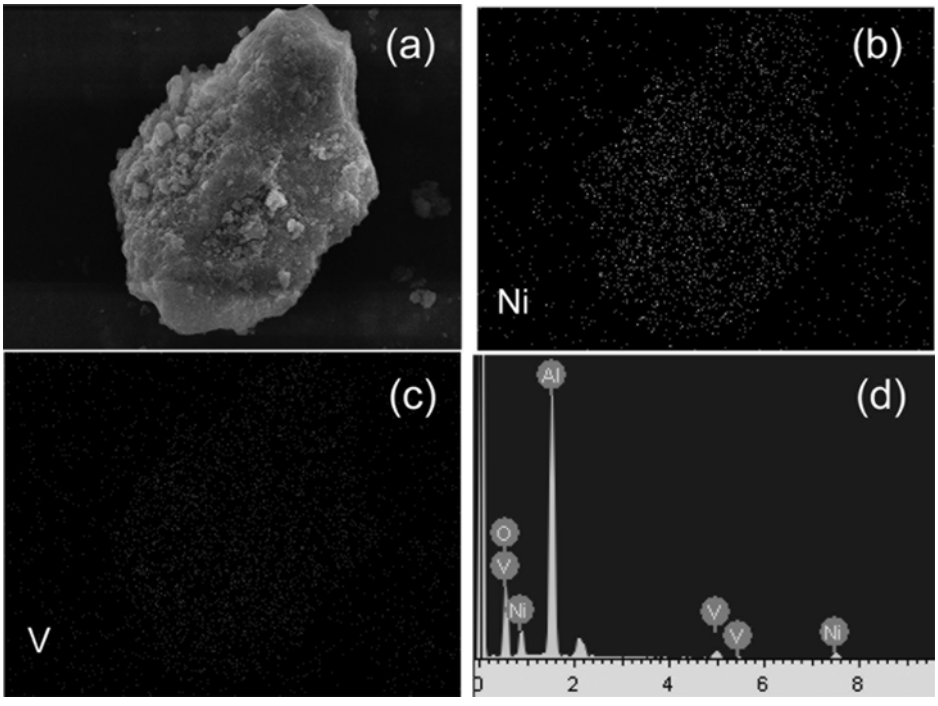

Fig. 4. SEM image of the reduced 20NA5V-CI (a), elemental mapping images of Ni (b), and V (c); Energy-dispersive X-ray spectroscopy (EDS) analysis of the sample (d).

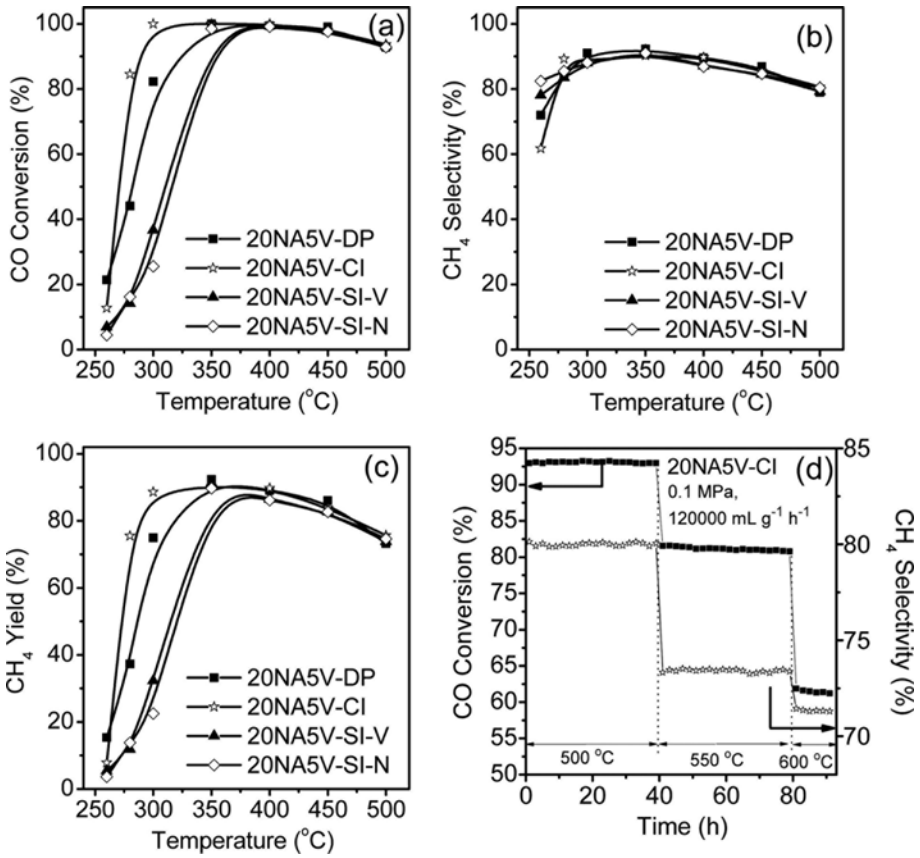

Fig. 5. Catalytic properties of the catalysts at 0.1 MPa, 120,000 mL g^{-1} h^{-1}: (a) CO conversion, (b) CH_4 selectivity, and (c) CH_4 yield; and 91h-lifetime test of 20NA5V-CI (d).

desorption from the single site chemisorption with low activation energy [19], while the peaks at high temperatures (243 and 478 °C) represent the desorption from the chemisorbed CO in bridge mode on two sites with high activation energy [19]. In short, we can conclude that the peak areas of the different catalysts are very close (20NA5V-CI≈20NA5V-DP>20NA5V-SI-V), while 20NA5V-SI-N has the smallest integral area due to the largest Ni particle size, indicating that the Ni particle size can have an effect on the CO adsorption. Thus, the enhanced CO sorption will lead to the higher activity of the 20NA5V-CI and 20NA5V-DP catalyst compared to 20NA5V-SI-V and 20NA5V-SI-N for CO methanation.

The TEM images of the reduced catalysts are shown in Fig. 3. A slight agglomeration of Ni particles can be observed over 20NA5V-SI-N and 20NA5V-SI-V, and there is no obvious Ni particle agglomeration in the reduced 20NA5V-CI and 20NA5V-DP. The average Ni particle size in 20NA5V-SI-N, 20NA5V-SI-V, 20NA5V-CI and 20NA5V-DP samples is 12.8, 7.2, 3.9 and 4.9 nm, respectively, in good agreement with the results of XRD in Table 1. Among all the catalysts, 20NA5V-CI has the smallest Ni particle size and the highest metallic Ni dispersion. In addition, the SEM image, elemental mappings and EDS of the reduced 20NA5V-CI are shown in Fig. 4, which confirm that Ni and vanadium promoter nanoparticles are homogeneously dispersed on the catalyst surface.

2. Catalytic Performance of the Catalysts

To investigate the effect of the preparation method on the catalytic activity, a CO methanation reaction was carried out in the temperature range of 260-500 °C at 0.1 MPa and at a weight hourly space velocity (WHSV) of 120,000 mL g^{-1} h^{-1}; the results are shown in Fig. 5(a)-(c). Clearly, the catalytic activities of 20NA5V-SI-N and 20NA5V-SI-V are similar and very poor, especially below 350 °C, and there is an obvious increase of the low-temperature activity for 20NA5V-CI and 20NA5V-DP. For example, on 20NA5V-CI, it even can reach 100% CO conversion at a reaction temperature as low as 300 °C. Furthermore, all the catalysts show similar activity above 400 °C because the reaction has reached thermodynamics equilibrium [20,21]. Moreover, there seems no obvious effect of preparation method on CH_4 selectivity. In all, the catalyst activity follows the sequence of 20NA5V-CI>20NA5V-DP>20NA5V-SI-V>20NA5V-SI-N, and the catalytic performance of Ni-V/Al_2O_3 catalysts is sensitive to their chemical and textural features, being closely related to the properties of the H_2 uptakes and metallic Ni dispersion. In addition, besides activity/selectivity, stability is also very important when considering the practical application for a heterogeneous catalyst. Therefore, a 91h-lifetime test for 20NA5V-CI was carried out at 500-600 °C, 0.1 MPa and a high WHSV of 120,000 mL g^{-1} h^{-1} (Fig. 5(d)). The CO conversion and CH_4 selectivity can remain stable during every time period from 500 to 600 °C, and only slightly decline of CO conversion can be observed at high temperatures (550 and 600 °C), suggesting its good stability at high temperatures and a high WHSV.

CONCLUSIONS

V-promoted Ni/Al_2O_3 catalysts were prepared by co-impregnation (CI) method, deposition precipitation (DP) method as well as two sequential impregnation (SI) methods with different impregnation sequence. A significant effect of preparation method on the catalytic performance was observed, and the catalyst prepared by co-impregnation method exhibited the best catalytic performance due to its largest H_2 uptake and highest metallic Ni dispersion. In a 91h-lifetime test conducted at high temperatures (500-600 °C), 0.1 MPa and WHSV of 120,000 mL g^{-1} h^{-1}, both CO conversion and CH_4 selectivity remained stable; thus this catalyst displays a high catalytic stability. This work demonstrates that the catalytic performance of the heterogeneous catalysts can be further enhanced by carefully regulating the preparation method.

ACKNOWLEDGEMENTS

The authors gratefully acknowledge the supports from the National Natural Science Foundation of China (No. 21476238), the National Basic Research Program (No. 2014CB744306), the National High Technology Research and Development Program 863 (No. SS2015AA050502), the Open Research Fund of State Key Laboratory of Multiphase Complex Systems (No. MPCS-2014-D-03), the Fund of State Key Laboratory of Multiphase complex systems (No. MPCS-2015-A-06) and "Strategic Priority Research Program" of the Chinese Academy of Sciences (Nos. XDA07010100 and XDA07010200).

REFERENCES

1. J. Kopyscinski, T. J. Schildhauer and S. M. A. Biollaz, *Fuel*, **89**, 1763 (2010).
2. Q. Liu, J. J. Gao, M. J. Zhang, H. F. Li, F. N. Gu, G. W. Xu, Z. Y. Zhong and F. B. Su, *RSC Adv.*, **4**, 16094 (2014).
3. Q. Liu, F. N. Gu, J. J. Gao, H. F. Li, G. W. Xu and F. B. Su, *J. Energy Chem.*, **23**, 761 (2014).
4. J. J. Gao, Q. Liu, F. N. Gu, B. Liu, Z. Y. Zhong and F. B. Su, *RSC Adv.*, **5**, 22759 (2015).
5. Y. Lee, H. Kim, H. Choi, D. W. Lee and K. Y. Lee, *Korean J. Chem. Eng.*, **32**, 2220 (2015).
6. J. J. Gao, C. M. Jia, J. Li, F. N. Gu, G. W. Xu, Z. Y. Zhong and F. B. Su, *Ind. Eng. Chem. Res.*, **51**, 10345 (2012).
7. C. M. Jia, J. J. Gao, J. Li, F. N. Gu, G. W. Xu, Z. Y. Zhong and F. B. Su, *Catal. Sci. Technol.*, **3**, 490 (2013).
8. J. J. Gao, C. M. Jia, J. Li, M. J. Zhang, F. N. Gu, G. W. Xu, Z. Y. Zhong and F. B. Su, *J. Energy Chem.*, **22**, 919 (2013).
9. A. M. Zhao, W. Y. Ying, H. T. Zhang, H. F. Ma and D. Y. Fang, *Catal. Commun.*, **17**, 34 (2012).
10. X. L. Yan, Y. Liu, B. R. Zhao, Z. Wang, Y. Wang and C. J. Liu, *Int. J. Hydrogen Energy*, **38**, 2283 (2013).
11. Q. Liu, F. N. Gu, X. P. Lu, Y. J. Liu, H. F. Li, Z. Y. Zhong, G. W. Xu and F. B. Su, *Appl. Catal. A*, **488**, 37 (2014).
12. X. P. Lu, F. N. Gu, Q. Liu, J. J. Gao, Y. J. Liu, H. F. Li, L. H. Jia, G. W. Xu, Z. Y. Zhong and F. B. Su, *Fuel Process. Technol.*, **135**, 34 (2015).
13. Q. Liu, J. J. Gao, F. N. Gu, X. P. Lu, Y. J. Liu, H. F. Li, Z. Y. Zhong, B. Liu, G. W. Xu and F. B. Su, *J. Catal.*, **326**, 127 (2015).
14. B. J. Kip, P. A. T. Smeets, J. Vangrondelle and R. Prins, *Appl. Catal.*, **33**, 181 (1987).
15. J. Liu, C. M. Li, F. Wang, S. He, H. Chen, Y. F. Zhao, M. Wei, D. G. Evans and X. Duan, *Catal. Sci. Technol.*, **3**, 2627 (2013).
16. S. Velu and S. Gangwal, *Solid State Ionics*, **177**, 803 (2006).
17. J. Sehested, S. Dahl, J. Jacobsen and J. R. Rostrup-Nielsen, *J. Phys. Chem. B*, **109**, 2432 (2005).
18. D. M. Stockwell, J. S. Chung and C. O. Bennett, *J. Catal.*, **112**, 135 (1988).
19. A. Tanksale, J. N. Beltramini, J. A. Dumesic and G. Q. Lu, *J. Catal.*, **258**, 366 (2008).
20. J. J. Gao, Y. L. Wang, Y. Ping, D. C. Hu, G. W. Xu, F. N. Gu and F. B. Su, *RSC Adv.*, **2**, 2358 (2012).
21. W. Kang and K. Lee, *Korean J. Chem. Eng.*, **30**, 1386 (2013).